Increasing the PV Hosting Capacity in Unbalanced Three-Phase Distribution Networks Through Reconfiguration with Closed-Loop Operation

Leonardo H. Macedo — *UNESP*, Ilha Solteira, Brazil, leohfmp@ieee.org
Renzo Vargas — *UFABC*, Santo André, Brazil, renzo@ieee.org
Juan M. Home-Ortiz — *UNESP*, Ilha Solteira, Brazil, juan.home@unesp.br
José R. S. Mantovani — *UNESP*, Ilha Solteira, Brazil, mant@dee.feis.unesp.br
Rubén Romero — *UNESP*, Ilha Solteira, Brazil, ruben.romero@unesp.br
João P. S. Catalão — *FEUP and INESC TEC*, Porto, Portugal, catalao@fe.up.pt

2021 IEEE International Conference on Environment and Electrical Engineering and 2021 IEEE Industrial and Commercial Power Systems Europe (EEEIC / I&CPS Europe) | 978-1-6654-3613-7/21/$31.00 ©2021 IEEE | DOI: 10.1109/EEEIC/ICPSEUROPE51590.2021.9611034

***Abstract*—This article presents a novel mixed-integer nonlinear linear programming (MINLP) model to increase the photovoltaic (PV) hosting capacity in unbalanced three-phase electrical distribution systems. The problem considers the optimal operation of capacitor banks and network reconfiguration with radial and closed-loop operation. The objective function maximizes the PV hosting capacity of the system. A set of linearization strategies are employed to convert the presented MINLP model into a mixed-integer linear programming (MILP) problem. By considering the MILP formulation, optimality is guaranteed by using off-the-shelf optimization solvers. Several tests are carried out using a 25-node unbalanced three-phase distribution system. When examining network reconfiguration with radial and closed-loop operation, the results demonstrate that the proposed formulation is effective in increasing the penetration of PV sources.**

***Keywords*—Closed-loop operation, hosting capacity, mixed-integer linear programming, network reconfiguration, unbalanced three-phase electrical distribution networks.**

NOMENCLATURE

Functions:

$\mathcal{V}$	Objective function of the problem
g	Real part of the load current
h	Imaginary part of the load current

Indices and sets:

φ	Index for linearization blocks
i, j	Indices for nodes
ij, ji	Indices for circuits
$f, \not{f}$	Indices for phases
k	Index for capacitor banks' (CBs) modules
s	Index for stochastic scenarios
Λ_B	Set of circuits
Λ_{CB}	Set of nodes with CBs
Λ_F	Set of phases $\{a, b, c\}$
Λ_N	Set of nodes
Λ_{PV}	Set of candidate nodes to install PV generation
Λ_S	Set of stochastic scenarios
Λ_{SS}	Set of substations (SSs) nodes

Parameters:

$\mathcal{B}_i^{CB}$	Susceptance of a CB module at a node
$e_{i,s}^{SS}$	CO_2 emissions intensity for SSs
$\overline{\iota}_{ij,f}$	Current capacity of a phase of a circuit
$\mathcal{N}^{LP}$	Number of basic loops allowed to be formed
$\mathcal{P}_{i,f,s}^{D}, \mathcal{Q}_{i,f,s}^{D}$	Active/reactive power demands
$\underline{\Upsilon}_i^{PV}, \overline{\Upsilon}_i^{PV}$	Power factor limits of a PV unit
$R_{ij,f,\not{f}}, X_{ij,f,\not{f}}$	Resistance/reactance between phases f and $\not{f}$
$\overline{\mathcal{S}}_i^{PV}$	Maximum capacity of PV generation that can be installed at a node
$\overline{\iota}_i^{SS}$	Current capacity of a SS
$\overline{\upsilon}, \underline{\upsilon}$	Maximum/minimum voltage magnitude limits
$\mathcal{N}_i^{CB}$	Number of CB modules installed at each phase of a node
Δ_s^T	Duration of a stochastic scenario
$\mathcal{G}_{i,s}^{PV}$	Generation factor of a PV generation unit
ξ	Total CO_2 emissions from the system
$\mathcal{C}_i$	Power curtailment limit for a PV unit
φ_f	Phase angle at phase f of a SS node
φ^+, φ^-	Maximum positive/negative variations of the phase angle around the reference
g^*, h^*	Values for g / h calculated at $(\upsilon_{i,f,s}^{R*}, \upsilon_{i,f,s}^{I*})$
$\upsilon_{i,f,s}^{R*}, \upsilon_{i,f,s}^{I*}$	Real/imaginary parts of the voltage magnitude estimated at a phase of a node
Φ	Number of blocks for the linearization

Continuous variables:

$\iota_{ij,f,s}^{SQ}$	Square of the current magnitude on a circuit
$\iota_{ij,f,s}^{R}, \iota_{ij,f,s}^{I}$	Real/imaginary components of the currents through each phase of a circuit
$\iota_{i,f,s}^{R^{SS}}, \iota_{i,f,s}^{I^{SS}}$	Real/imaginary components of the currents injected by a SS
$\iota_{i,f,s}^{R^{PV}}, \iota_{i,f,s}^{I^{PV}}$	Real/imaginary components of the currents injected by a PV unit
$\iota_{i,f,k,s}^{R^{CB}}, \iota_{i,f,k,s}^{I^{CB}}$	Real/imaginary components of the currents injected by a CB module
$\hat{\iota}_{i,f,s}^{R^{CB}}, \hat{\iota}_{i,f,s}^{I^{CB}}$	Real/imaginary components of the currents injected by a CB
$\iota_{i,f,s}^{R^{D}}, \iota_{i,f,s}^{I^{D}}$	Real/imaginary components of the demanded current at a node
$\mathcal{S}_i^{PV}$	Installed capacity of PV generation at a node
$\upsilon_{i,f,s}^{R}, \upsilon_{i,f,s}^{I}$	Real/imaginary components of the nodal voltages
$\tau_{ij,f,s}^{R}, \tau_{ij,f,s}^{I}$	Slack variables for the calculation of the voltage drop on a circuit
$\mathscr{p}_{ij}$	Artificial flow on a circuit
$\mathscr{g}_i$	Artificial generation at SS nodes
$\mathcal{P}_{i,s}^{PV}, \mathcal{Q}_{i,s}^{PV}$	Active/reactive power generations of PV units
$\mathcal{P}_{i,s}^{C}$	Power curtailment for a PV generation unit
$\gamma_{ij,f,\varphi,s}^{R}, \gamma_{ij,f,\varphi,s}^{I}$	Values of the blocks of the linearization
$\iota_{ij,f,s}^{R+}, \iota_{ij,f,s}^{R-}$	Positive component of the real current through a phase of a circuit
$\iota_{ij,f,s}^{I+}, \iota_{ij,f,s}^{I-}$	Negative component of the real current through a phase of a circuit

Binary variables:

x_{ij}^{SW}	Operational state of a circuit
$z_{i,f,k}^{CB}$	Operational state of CBs modules

This work was supported by the Coordination for the Improvement of Higher Education Personnel (CAPES) – Finance Code 001, the Brazilian National Council for Scientific and Technological Development (CNPq), grants 305852/2017-5 and 304726/2020-6, the São Paulo Research Foundation (FAPESP), under grants 2015/21972-6, 2018/20355-1, 2019/01841-5, and 2019/23755-3, and by ENEL under the grant PEE-00390-1062/2017 - P&D-00390-1083-2020_UFABC, ANEEL 001-2016.

J. P. S. Catalão acknowledges the support by FEDER funds through COMPETE 2020 and by Portuguese funds through FCT, under POCI-01-0145-FEDER-029803 (02/SAICT/2017).

I. Introduction

The constant growth of environmental concerns and technological progress has motivated the integration of distributed generation (DG) based on renewable energy sources (RES) in electric power systems [1]. However, because of the intermittency of RES, the output of DG presents significant uncertainty, impacting the normal operation of electric systems. This calls for studies to evaluate how much of these new energy sources can be integrated into electric power systems.

The hosting capacity problem aims to determine the capacity of an electric power system to accommodate new energy sources without violating technical and operational constraints [1]. In distribution systems, the introduction of these new energy sources is a challenging task since conventional distribution systems are planned considering the primary substation (SS) as the only energy source, with unidirectional power flow from the SS to the final consumer. Depending on the location and level of penetration, RES introduction is restricted by operational constraints, including thermal and voltage limits [2]. To overcome these limitations, the standard solution has been the application of grid reinforcement strategies, however, this approach is slow and costly [1]. Thus, other alternatives should be explored to adequate and improve distribution systems operation for improving the hosting capacity.

Network reconfiguration is a major strategy to improve distribution systems' operation. It consists of changing the state of sectional and tie switches to modify the topology of the system [2]. In [2], the potential of network reconfiguration to improve hosting capacity in a 33-node balanced distribution system is assessed. The problem is formulated as a mixed-integer nonlinear model to maximize the DG hosting capacity considering thermal and voltage constraints. In [1], a multiperiod network reconfiguration strategy is proposed to increase the hosting capacity of distribution systems considering the uncertainty of renewable generation. The problem is formulated as a nonlinear, nondifferentiable integer optimization problem and solved using a hybrid particle swarm optimization algorithm. In [3], the impact of network reconfiguration is analyzed for improving the photovoltaic (PV) hosting capacity using a binary particle swarm optimization algorithm. The formulation of the problem considers minimizing voltage violations associated with increasing solar penetration in a 37-node unbalanced three-phase test system.

Distribution systems are planned in meshed structures and are usually operated in radial topologies to facilitate protection coordination and reduce short-circuit currents [4]. A meshed structure allows reconfiguration procedures in normal state and reconnection of de-energized loads after a permanent fault. In the literature, works have considered closed-loop operation for reducing technical losses [5], improve reliability indices in normal operation [6], and the possibility of reconnecting more loads to primary feeders during the restorative operation state [7]. In [8], closed-loop topologies are considered for RES integration in a 119-node balanced distribution system. In [9], network reconfiguration with a relaxed radiality constraint is proposed for increasing the hosting capacity in distribution systems. A modified genetic algorithm is employed to solve the problem in a 69-node balanced system.

In the literature, other approaches have been considered for improving hosting capacity. In [10], the impact of active system management schemes is analyzed in the PV hosting capacity of distribution systems. In [11], a robust optimization method is proposed for evaluating the maximum hosting capacity. Voltage control and reactive power compensation are also considered for improving the capability of the distribution systems to accommodate DG. In [12], active distribution system management including switching capacitor banks (CBs), controllable switches, and smart PV inverters are considered for maximizing PV hosting capacity. The problem is formulated as a mixed-integer nonlinear optimization model and solved using a genetic algorithm-based approach.

For enhancing the maximum penetration of PV generation in distribution systems, this study considers network reconfiguration procedures and switchable CBs adjustments. Unlike the majority of works in the literature, we are considering the possibility of allowing closed-loop operation to maximize the PV hosting capacity in unbalanced three-phase distribution systems. The problem is formulated as a mixed-integer nonlinear programming (MINLP) model and converted into a mixed-integer linear programming (MILP) model using linearization strategies. A stochastic scenario-based formulation is used to handle the uncertainties of PV generation. The objective function of the proposed model is defined as maximizing the penetration of PV generation in distribution systems. To validate the proposed formulation, several tests are performed in a 25-node unbalanced three-phase distribution system.

The main contributions of this work are as follows:

- A novel stochastic-programming-based model for identifying the optimal operation of unbalanced three-phase distribution systems, which allows for closed-loop topology and CBs adjustments to enhance PV hosting capacity;
- The resulting MINLP problem is recast into a MILP formulation, which can be effectively solved by optimization solvers, in order to guarantee convergence to the optimal solution of the problem.

The benefits of the proposed approach include improving the efficiency of the system and reducing the associated CO_2 emissions.

The remainder of this work is divided into the following sections: Section II introduces the proposed formulation for the problem; Section III presents the results for the tests performed using a 25-node unbalanced three-phase distribution system; finally, the conclusions of the work are presented in Section IV.

II. Mathematical Formulation

The proposed MINLP formulation for the problem is presented below. Then, the linearizations of the nonlinear constraints are introduced in the second part of this section.

A. Objective Function

The model maximizes the PV hosting capacity of the system. Equation (1) presents the objective function $\mathcal{V}$ of the problem.

$$\text{maximize}\, \mathcal{V} = \sum_{i \in \Lambda_{PV}} \mathcal{S}_i^{PV} \tag{1}$$

The objective function (1) maximizes the sum of the PV units capacity in the system.

B. Operational Constraints of the System

The operation of the system is represented by (2)–(9), expressed in terms of currents in rectangular coordinates.

$$\sum_{ji\in\Lambda_B} \iota^R_{ji,f,s} - \sum_{ij\in\Lambda_B} \iota^R_{ij,f,s} + \iota^{R^{SS}}_{i,f,s} + \iota^{R^{PV}}_{i,f,s} + \hat{\iota}^{R^{CB}}_{i,f,s} = \iota^{R^D}_{i,f,s} \tag{2}$$

$$\sum_{ji\in\Lambda_B} \iota^I_{ji,f,s} - \sum_{ij\in\Lambda_B} \iota^I_{ij,f,s} + \iota^{I^{SS}}_{i,f,s} + \iota^{I^{PV}}_{i,f,s} + \hat{\iota}^{I^{CB}}_{i,f,s} = \iota^{I^D}_{i,f,s} \tag{3}$$

$$\iota^{R^D}_{i,f,s} = \frac{\mathcal{P}^D_{i,f,s}\upsilon^R_{i,f,s} + \mathcal{Q}^D_{i,f,s}\upsilon^I_{i,f,s}}{\left(\upsilon^R_{i,f,s}\right)^2 + \left(\upsilon^I_{i,f,s}\right)^2} \tag{4}$$

$$\iota^{I^D}_{i,f,s} = \frac{\mathcal{P}^D_{i,f,s}\upsilon^I_{i,f,s} - \mathcal{Q}^D_{i,f,s}\upsilon^R_{i,f,s}}{\left(\upsilon^R_{i,f,s}\right)^2 + \left(\upsilon^I_{i,f,s}\right)^2} \tag{5}$$

$$\forall i \in \Lambda_N, f \in \Lambda_F, s \in \Lambda_S$$

$$\upsilon^R_{i,f,s} - \upsilon^R_{j,f,s} + \tau^R_{ij,f,s} = \sum_{\not{f}\in\Lambda_F} \left(R_{ij,f,\not{f}}\iota^R_{ij,\not{f},s} - X_{ij,f,\not{f}}\iota^I_{ij,\not{f},s}\right) \tag{6}$$

$$\upsilon^I_{i,f,s} - \upsilon^I_{j,f,s} + \tau^I_{ij,f,s} = \sum_{\not{f}\in\Lambda_F} \left(X_{ij,f,\not{f}}\iota^R_{ij,\not{f},s} + R_{ij,f,\not{f}}\iota^I_{ij,\not{f},s}\right) \tag{7}$$

$$\left|\tau^R_{ij,f,s}\right| \le 2\overline{\upsilon}(1 - x^{SW}_{ij}) \tag{8}$$

$$\left|\tau^I_{ij,f,s}\right| \le 2\overline{\upsilon}(1 - x^{SW}_{ij}) \tag{9}$$

$$\forall ij \in \Lambda_B, f \in \Lambda_F, s \in \Lambda_S$$

Constraints (2) and (3) represent the application of Kirchhoff's current law to the system in each scenario and provide the nodal balance equations for the real and imaginary components of the currents, respectively. The real and imaginary components of the three-phase current demanded by the load at each node in each scenario are calculated by constraints (4) and (5). The systematic application of Kirchhoff's voltage law to the system is represented by constraints (6)–(9). The slack variables $\tau^R_{ij,f,s}$ and $\tau^I_{ij,f,s}$ are calculated using (8) and (9) depending on the states of the switches.

C. Physical and Operational Limits of the System

Constraints (10)–(16) are the physical and operational limits of the system.

$$(\iota^R_{ij,f,s})^2 + (\iota^I_{ij,f,s})^2 \le \bar{\iota}^2_{ij,f} x^{SW}_{ij} \quad \forall ij \in \Lambda_B, f \in \Lambda_F, s \in \Lambda_S \tag{10}$$

$$\left|\iota^R_{ij,f,s}\right| \le \overline{\iota}_{ij,f} x^{SW}_{ij} \quad \forall ij \in \Lambda_B, f \in \Lambda_F, s \in \Lambda_S \tag{11}$$

$$\left|\iota^I_{ij,f,s}\right| \le \overline{\iota}_{ij,f} x^{SW}_{ij} \quad \forall ij \in \Lambda_B, f \in \Lambda_F, s \in \Lambda_S \tag{12}$$

$$\underline{\upsilon}^2 \le (\upsilon^R_{i,f,s})^2 + (\upsilon^I_{i,f,s})^2 \le \overline{\upsilon}^2 \quad \forall i \in \Lambda_N, f \in \Lambda_F, s \in \Lambda_S \tag{13}$$

$$-\overline{\upsilon} \le \upsilon^R_{i,f,s} \le \overline{\upsilon} \quad \forall i \in \Lambda_N, f \in \Lambda_F, s \in \Lambda_S \tag{14}$$

$$-\overline{\upsilon} \le \upsilon^I_{i,f,s} \le \overline{\upsilon} \quad \forall i \in \Lambda_N, f \in \Lambda_F, s \in \Lambda_S \tag{15}$$

$$\left(\iota^{R^{SS}}_{i,f,s}\right)^2 + \left(\iota^{I^{SS}}_{i,f,s}\right)^2 \le (\bar{\iota}^{SS}_i)^2 \quad \forall i \in \Lambda_{SS}, f \in \Lambda_F, s \in \Lambda_S \tag{16}$$

Constraints (10)–(12) specify the current capacity, real component, and imaginary component limits for the current on each phase of the circuits based on the switch states. The voltage magnitude limit for each phase of the nodes is constrained by (13); the real and imaginary components of the voltage for each phase at each node are constrained by (14) and (15), respectively. Finally, each phase of the SSs has a current capacity limit defined by (16).

D. Operation of CBs

The operation of the CBs is modeled in (17)–(20).

$$\hat{\iota}^{R^{CB}}_{i,f,s} = \sum_{k=1}^{\mathcal{N}^{CB}_i} \iota^{R^{CB}}_{i,f,k,s} \quad \forall i \in \Lambda_{CB}, f \in \Lambda_F, s \in \Lambda_S \tag{17}$$

$$\hat{\iota}^{I^{CB}}_{i,f,s} = \sum_{k=1}^{\mathcal{N}^{CB}_i} \iota^{I^{CB}}_{i,f,k,s} \quad \forall i \in \Lambda_{CB}, f \in \Lambda_F, s \in \Lambda_S \tag{18}$$

$$\iota^{R^{CB}}_{i,f,k,s} = \mathcal{B}^{CB}_i \upsilon^I_{i,f,s} z^{CB}_{i,f,k} \tag{19}$$

$$\iota^{I^{CB}}_{i,f,k,s} = -\mathcal{B}^{CB}_i \upsilon^R_{i,f,s} z^{CB}_{i,f,k} \tag{20}$$

$$\forall i \in \Lambda_{CB}, f \in \Lambda_F, k \in \{1, \cdots, \mathcal{N}^{CB}_{ij}\}, s \in \Lambda_S$$

Constraints (17) and (18) determine the total real and imaginary components of the currents injected by a CB at each phase and node, respectively, while (19) and (20) calculate the real and imaginary components of the current injected by each CB module at each phase, respectively. It is worth noting that the CBs in each phase are controlled separately.

E. Topological Constraints

Artificial demands that must be fulfilled at all nodes are used by (21)–(24) to control the network's connectivity and the maximum number of basic loops that may be formed.

$$|\Lambda_N| - |\Lambda_{SS}| \le \sum_{ij\in\Lambda_B} x^{SW}_{ij} \le |\Lambda_N| - |\Lambda_{SS}| + \mathcal{N}^{LP} \tag{21}$$

$$\sum_{ji\in\Lambda_B} \boldsymbol{\mathcal{p}}_{ji} - \sum_{ij\in\Lambda_B} \boldsymbol{\mathcal{p}}_{ij} + \boldsymbol{\mathcal{g}}_i = 1 \quad \forall i \in \Lambda_N \tag{22}$$

$$\left|\boldsymbol{\mathcal{p}}_{ij}\right| \le |\Lambda_N| x^{SW}_{ij} \quad \forall ij \in \Lambda_B \tag{23}$$

$$0 \le \boldsymbol{\mathcal{g}}_i \le |\Lambda_N| \quad \forall i \in \Lambda_{SS} \tag{24}$$

Constraint (21) is used to restrict the maximum number of basic loops in the network, whereas constraints (22)–(24) guarantee network connection, i.e., that each node in the network must have a path to a SS. Note that, $\boldsymbol{\mathcal{g}}_i = 0$ for the load nodes.

F. PV Hosting Capacity

The operation and investment constraints in PV units are formulated in (25)–(32). Equation (33) calculates the total emissions from the system.

$$\mathcal{P}^{PV}_{i,s}/3 = \upsilon^R_{i,f,s}\iota^{R^{PV}}_{i,f,s} + \upsilon^I_{i,f,s}\iota^{I^{PV}}_{i,f,s} \tag{25}$$

$$\mathcal{Q}^{PV}_{i,s}/3 = -\upsilon^R_{i,f,s}\iota^{I^{PV}}_{i,f,s} + \upsilon^I_{i,f,s}\iota^{R^{PV}}_{i,f,s} \tag{26}$$

$$\forall i \in \Lambda_{PV}, f \in \Lambda_F, s \in \Lambda_S$$

$$(\mathcal{P}^{PV}_{i,s})^2 + (\mathcal{Q}^{PV}_{i,s})^2 \le (\mathcal{S}^{PV}_i)^2 \quad \forall i \in \Lambda_{PV}, s \in \Lambda_S \tag{27}$$

$$-\mathcal{P}^{PV}_{i,s}\tan(\cos^{-1}(\underline{\Upsilon}^{PV}_i)) \le \mathcal{Q}^{PV}_{i,s} \le \mathcal{P}^{PV}_{i,s}\tan\left(\cos^{-1}\left(\overline{\Upsilon}^{PV}_i\right)\right) \tag{28}$$

$$\forall i \in \Lambda_{PV}, s \in \Lambda_S$$

$$\mathcal{P}^{PV}_{i,s} = \mathcal{G}^{PV}_{i,s}\mathcal{S}^{PV}_i - \mathcal{P}^C_{i,s} \quad \forall i \in \Lambda_{PV}, s \in \Lambda_S \tag{29}$$

$$0 \le \mathcal{P}^C_{i,s} \le \mathcal{G}^{PV}_{i,s}\mathcal{S}^{PV}_i \quad \forall i \in \Lambda_{PV}, s \in \Lambda_S \tag{30}$$

$$0 \le \mathcal{S}^{PV}_i \le \overline{\mathcal{S}}^{PV}_i \quad \forall i \in \Lambda_{PV} \tag{31}$$

$$\sum_{s\in\Lambda_S} \Delta^T_s \mathcal{P}^C_{i,s} \le \mathcal{C}_i \sum_{s\in\Lambda_S} \Delta^T_s \mathcal{G}^{PV}_{i,s}\overline{\mathcal{S}}^{PV}_i \quad \forall i \in \Lambda_{PV} \tag{32}$$

$$\xi = \sum_{i\in\Lambda_{SS}} \sum_{f\in\Lambda_F} \sum_{s\in\Lambda_S} \Delta^T_s e^{SS}_{i,s}\left(\upsilon^R_{i,f,s}\iota^{R^{SS}}_{i,f,s} + \upsilon^I_{i,f,s}\iota^{I^{SS}}_{i,f,s}\right) \tag{33}$$

In each scenario s, constraints (25) and (26) define the active and reactive power injected by the PV unit at node i. The apparent power limit of the PV units is represented by constraint (27) and the power factor limits of the PV units are defined in (28). Constraint (29) restricts the PV unit's active power injection at node i to the generating capacity in scenario s. The active power curtailment is limited by (30). The maximum PV capacity that may be installed at a node is limited by constraint (31). The total amount of energy that can be

curtailed is limited by (32). Finally, the system's total CO_2 emissions are determined in (33).

In the proposed model, the objective function (1) is linear, as well constraints (2), (3), (6)–(9), (11), (12), (14), (15), (17), (18), (21)–(24), and (28)–(32). Constraints (4), (5), (10), (13), (16), (19), (20), and (25)–(27) are nonlinear. Due to the presence of the binary variables x_{ij}^{SW} and $z_{i,f,k}^{CB}$, the resulting formulation is an MINLP model, which is difficult to solve directly. The following subsection will present linear formulations to the nonlinear constraints.

G. Linearization of the Nonlinear Constraints

The current demanded by the loads, presented in (2) and (3) is linearized as presented in (34)–(37) [13].

$$g(v_{i,f,s}^R, v_{i,f,s}^I) = \frac{\mathcal{P}_{i,f,s}^D v_{i,f,s}^R + \mathcal{Q}_{i,f,s}^D v_{i,f,s}^I}{\left(v_{i,f,s}^R\right)^2 + \left(v_{i,f,s}^I\right)^2} \tag{34}$$

$$h(v_{i,f,s}^R, v_{i,f,s}^I) = \frac{\mathcal{P}_{i,f,s}^D v_{i,f,s}^I - \mathcal{Q}_{i,f,s}^D v_{i,f,s}^R}{\left(v_{i,f,s}^R\right)^2 + \left(v_{i,f,s}^I\right)^2} \tag{35}$$

$$\iota_{i,f,s}^{R^D} \approx g^* + \left.\frac{\partial g}{\partial v_{i,f,s}^R}\right|^* (v_{i,f,s}^R - v_{i,f,s}^{R*}) + \left.\frac{\partial g}{\partial v_{i,f,s}^I}\right|^* (v_{i,f,s}^I - v_{i,f,s}^{I*}) \tag{36}$$

$$\iota_{i,f,s}^{I^D} \approx h^* + \left.\frac{\partial h}{\partial v_{i,f,s}^R}\right|^* (v_{i,f,s}^R - v_{i,f,s}^{R*}) + \left.\frac{\partial h}{\partial v_{i,f,s}^I}\right|^* (v_{i,f,s}^I - v_{i,f,s}^{I*}) \tag{37}$$

$$\forall i \in \Lambda_N, f \in \Lambda_F, s \in \Lambda_S$$

Constraints (34) and (35) define the auxiliary functions g and h, obtained from the right hand side of (4) and (5), respectively. The first-order terms of the Taylor series expansion of g and h at the estimated values for the real and imaginary parts of the nodal voltages, $v_{i,f,s}^{R*}$ and $v_{i,f,s}^{I*}$, are represented in constraints (36) and (37), respectively.

Constraint (10) is replaced by the linear equivalent (38), while the squared value of the current magnitude at each phase of each circuit, in each scenario, is calculated using the piecewise linearization (39)–(45) [13].

$$0 \le \iota_{ij,f,s}^{SQ} \le \bar{\iota}_{ij,f}^2 x_{ij}^{SW} \qquad \forall ij \in \Lambda_B, f \in \Lambda_F, s \in \Lambda_S \tag{38}$$

$$\iota_{ij,f,s}^{SQ} \approx \sum_{\varphi=1}^{\Phi} \frac{(2\varphi-1)\bar{\iota}_{ij,f}}{\Phi} (\gamma_{ij,f,\varphi,s}^R + \gamma_{ij,f,\varphi,s}^I) \tag{39}$$

$$\iota_{ij,f,s}^R = \iota_{ij,f,s}^{R+} - \iota_{ij,f,s}^{R-} \qquad \forall ij \in \Lambda_B, f \in \Lambda_F, s \in \Lambda_S \tag{40}$$

$$\iota_{ij,f,s}^I = \iota_{ij,f,s}^{I+} - \iota_{ij,f,s}^{I-} \qquad \forall ij \in \Lambda_B, f \in \Lambda_F, s \in \Lambda_S \tag{41}$$

$$\iota_{ij,f,s}^{R+} + \iota_{ij,f,s}^{R-} = \sum_{\varphi=1}^{\Phi} \gamma_{ij,f,\varphi,s}^R \qquad \forall ij \in \Lambda_B, f \in \Lambda_F, s \in \Lambda_S \tag{42}$$

$$\iota_{ij,f,s}^{I+} + \iota_{ij,f,s}^{I-} = \sum_{\varphi=1}^{\Phi} \gamma_{ij,f,\varphi,s}^I \qquad \forall ij \in \Lambda_B, f \in \Lambda_F, s \in \Lambda_S \tag{43}$$

$$0 \le \gamma_{ij,f,\varphi,s}^R \le \bar{\iota}_{ij,f}/\Phi \tag{44}$$

$$0 \le \gamma_{ij,f,\varphi,s}^I \le \bar{\iota}_{ij,f}/\Phi \tag{45}$$

$$\forall ij \in \Lambda_B, f \in \Lambda_F, \varphi \in \{1, \cdots, \Phi\}, s \in \Lambda_S$$

As presented in [13], the nodal voltage magnitude constraints (13) can be linearized by defining maximum positive and negative variations, φ^+ and φ^-, around the reference angle of each phase, φ_f. The set of constraints (46)–(50) is an approximation for (13). The inequality symbols used in these constraints are shown in Table I, for each phase. Also, it is assumed that φ^+ and φ^- are lower than 30°.

TABLE I
SYMBOLS FOR CONSTRAINTS (46)–(50)

Constraint	$f = a$	$f = b$	$f = c$
(46)	$\geqq$	$\leqq$	$\geqq$
(47)	$\leqq$	$\geqq$	$\leqq$
(48)	$\geqq$	$\geqq$	$\leqq$
(49)	$\leqq$	$\geqq$	$\geqq$
(50)	$\geqq$	$\leqq$	$\leqq$

$$v_{i,f,s}^I \geqq \frac{\sin(\varphi_f + \varphi^+) - \sin(\varphi_f - \varphi^-)}{\cos(\varphi_f + \varphi^+) - \cos(\varphi_f - \varphi^-)} [v_{i,f,s}^R - \underline{v}\cos(\varphi_f + \varphi^+)] + \underline{v}\sin(\varphi_f + \varphi^+) \tag{46}$$

$$v_{i,f,s}^I \leqq \frac{\sin(\varphi_f + \varphi^+) - \sin(\varphi_f)}{\cos(\varphi_f + \varphi^+) - \cos(\varphi_f)} [v_{i,f,s}^R - \overline{v}\cos(\varphi_f)] + \overline{v}\sin(\varphi_f) \tag{47}$$

$$v_{i,f,s}^I \leqq \frac{\sin(\varphi_f - \varphi^-) - \sin(\varphi_f)}{\cos(\varphi_f - \varphi^-) - \cos(\varphi_f)} [v_{i,f,s}^R - \overline{v}\cos(\varphi_f)] + \overline{v}\sin(\varphi_f) \tag{48}$$

$$v_{i,f,s}^I \leqq v_{i,f,s}^R \tan(\varphi_f + \varphi^+) \tag{49}$$

$$v_{i,f,s}^I \leqq v_{i,f,s}^R \tan(\varphi_f - \varphi^-) \tag{50}$$

$$\forall i \in \Lambda_N, f \in \Lambda_F, s \in \Lambda_S$$

The current injection by the SSs, (16), is linearized as shown in (51) and (52).

$$\left|\iota_{i,f,s}^{R^{SS}}\right| \le \bar{\iota}_i^{SS} \qquad \forall i \in \Lambda_{SS}, f \in \Lambda_F, s \in \Lambda_S \tag{51}$$

$$\left|\iota_{i,f,s}^{I^{SS}}\right| \le \bar{\iota}_i^{SS} \qquad \forall i \in \Lambda_{SS}, f \in \Lambda_F, s \in \Lambda_S \tag{52}$$

The nonlinear terms related to the operation of CBs, (19) and (20), can be represented by the disjunctive formulation (53)–(56).

$$\left|\frac{\iota_{i,f,k,s}^{R^{CB}}}{\mathcal{B}_i^{CB}} - v_{i,f,s}^I\right| \le \overline{v}(1 - z_{i,f,k}^{CB}) \tag{53}$$

$$\left|\iota_{i,f,k,s}^{R^{CB}}\right| \le \overline{v}\mathcal{B}_i^{CB} z_{i,f,k}^{CB} \tag{54}$$

$$\left|\frac{\iota_{i,f,k,s}^{I^{CB}}}{\mathcal{B}_i^{CB}} + v_{i,f,s}^R\right| \le \overline{v}(1 - z_{i,f,k}^{CB}) \tag{55}$$

$$\left|\iota_{i,f,k,s}^{I^{CB}}\right| \le \overline{v}\mathcal{B}_i^{CB} z_{i,f,k}^{CB} \tag{56}$$

$$\forall i \in \Lambda_{CB}, f \in \Lambda_F, k \in \{1, \cdots, \mathcal{N}_{ij}^{CB}\}, s \in \Lambda_S$$

Note that, in these constraints, when $z_{i,f,k}^{CB} = 1$, then $\iota_{i,f,k,s}^{R^{CB}} = \mathcal{B}_i^{CB} v_{i,f,s}^I$ and $\iota_{i,f,k,s}^{I^{CB}} = -\mathcal{B}_i^{CB} v_{i,f,s}^R$. When $z_{i,f,k}^{CB} = 0$, $\iota_{i,f,k,s}^{R^{CB}} = \iota_{i,f,k,s}^{I^{CB}} = 0$, and the imaginary and real components of the voltage are adequately bounded in (53) and (55), respectively.

The nonlinear constraints that represent the operation of PV units, (25)–(27), are linearized in (57)–(63).

$$\mathcal{P}_{i,s}^{PV}/3 \approx v_{i,f,s}^{R*} \iota_{i,f,s}^{R^{PV}} + v_{i,f,s}^{I*} \iota_{i,f,s}^{I^{PV}} \tag{57}$$

$$\mathcal{Q}_{i,s}^{PV}/3 \approx -v_{i,f,s}^{R*} \iota_{i,f,s}^{I^{PV}} + v_{i,f,s}^{I*} \iota_{i,f,s}^{R^{PV}} \tag{58}$$

$$\forall i \in \Lambda_{PV}, f \in \Lambda_F, s \in \Lambda_S$$

$$0 \le \mathcal{P}_{i,s}^{PV} \le \mathcal{S}_i^{PV} \qquad \forall i \in \Lambda_{PV}, s \in \Lambda_S \tag{59}$$

$$\left|\mathcal{Q}_{i,s}^{PV}\right| \le \mathcal{S}_i^{PV} \qquad \forall i \in \Lambda_{PV}, s \in \Lambda_S \tag{60}$$

$$\left|\mathcal{Q}_{i,s}^{PV}\right| \le \sqrt{2}\mathcal{S}_i^{PV} - \mathcal{P}_{i,s}^{PV} \qquad \forall i \in \Lambda_{PV}, s \in \Lambda_S \tag{61}$$

$$\left|\mathcal{Q}_{i,s}^{PV}\right| \le \frac{1}{\sin\left(\frac{\pi}{8}\right)} \mathcal{S}_i^{PV} - \tan\left(\frac{3\pi}{8}\right) \mathcal{P}_{i,s}^{PV} \qquad \forall i \in \Lambda_{PV}, s \in \Lambda_S \tag{62}$$

$$\left|\mathcal{Q}_{i,s}^{PV}\right| \le \frac{1}{\sin\left(\frac{3\pi}{8}\right)} \mathcal{S}_i^{PV} - \tan\left(\frac{\pi}{8}\right) \mathcal{P}_{i,s}^{PV} \qquad \forall i \in \Lambda_{PV}, s \in \Lambda_S \tag{63}$$

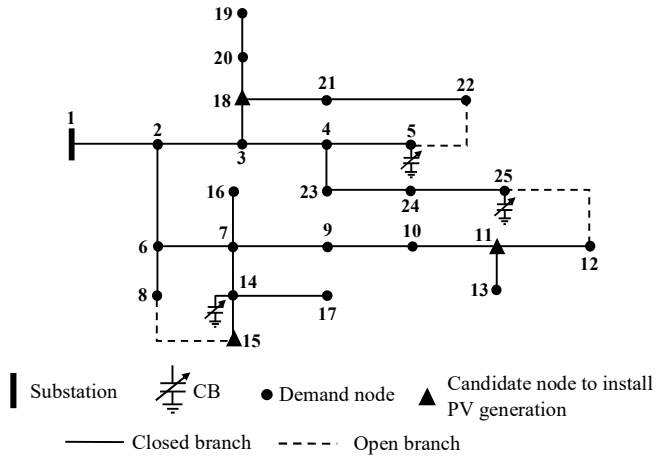

Fig. 1 Initial configuration of the 25-node distribution network.

Constraints (57) and (58) use the real and imaginary components of an estimated voltage at each phase of each node. Constraints (59)–(63) are a polyhedral approximation of (27).

The resulting formulation is a MILP problem, which can be efficiently solved by optimization solvers:

$$\text{maximize } (1)$$

Subject to: (2), (3), (6)–(9), (11), (12), (14), (15), (17), (18), (21)–(24), (28)–(32), and (34)–(63).

III. Tests and Results

The proposed model is validated using the 4.16 kV 25-node unbalanced three-phase system depicted in Fig. 1 [13]. Three switchable CBs with two modules of 100 kVAr per phase are installed at nodes 5, 14, and 25. Nodes 11, 15, and 18 are candidates for PV generation installation, with $\underline{\Upsilon}_i^{PV} = \overline{\Upsilon}_i^{PV} = 0.85$ and $\mathcal{C}_i = 10\%$. For the SS, $e_{i,s}^{SS} = 2.17$ kg CO_2/kWh. The maximum and minimum voltage limits are 1.05 p.u. and 0.95 p.u., respectively.

A one-year operation horizon is examined. Historical data from the seasons [14] is utilized to represent load behavior and solar irradiation, and the *k-means* clustering technique is used to limit it to an acceptable set of 24 scenarios using the procedure outlined in [15].

The proposed formulation was implemented in AMPL [16] and solved with the commercial solver CPLEX v20.1.0 [17] on a computer with a 3.2 GHz Intel® Core™ i7–8700 processor and 32 GB of RAM.

A. Study Cases

The following four cases are considered while maximizing the PV hosting capacity of the system:

I. Without taking into account network reconfiguration (the closed switches of the initial configuration of the network cannot be opened) and without considering the adjustments of the CBs, i.e., they are fixed at their initial states;
II. Disregarding network reconfiguration and considering the optimal operation of CBs;
III. Considering network reconfiguration and disregarding the optimal operation of CBs;
IV. Considering both network reconfiguration and the optimal operation of CBs.

The radial and closed-loop operation of the system is examined in all cases.

B. Discussion of the Results

Tables II–V show the total PV generation hosting capacity for the 25-node system in Cases I–IV, respectively. These tables also show the maximum capacity for PV generation integration at nodes 11, 15, and 18, as well as the network configuration, indicated by the open switches, and estimated CO_2 emissions.

Table II shows that the maximum PV generation that can be incorporated into the 25-node system is 13,816.14 kW, based on the network's initial radial configuration and without accounting for changes in CBs operation. It can be also seen that the PV generation installed increases by 4.45% after closing the switch of circuit 15-8 and allowing one loop in the system. The maximum PV penetration of 15,073.42 kW is reached by closing the switches of circuits 15-8 and 12-25, allowing two loops in the topology.

For the case considering adjustments of CBs operation but avoiding network reconfiguration, Table III shows that the adjustments of CBs operation allow increasing the PV generation capacity in 2.43% in relation to the initial radial configuration. Like in Case I, the maximum capacity of PV generation installed in the system is reached with the same two loops formed, however, the adjustments of CBs allow increasing by 3.19% the PV generation installed in relation to the solution of Case I with two loops.

Table IV presents the obtained results allowing the network reconfiguration without adjustments of CBs. For a radial configuration, the PV generation penetration can be increased by 7.07% to 14,793.34 kW, in relation to the initial radial configuration. On the other hand, this solution allows to install 4.53% more PV generation than the radial solution obtained in Case II. In this case, the loop formation allows increasing the PV penetration up to 3.48% and 3.74% when one and two loops are considered, respectively, in relation to the radial solution.

Finally, Table V shows that, in comparison to the initial radial topology, PV generation penetration can be increased by 8.36%, reaching 14,971.44 kW when radial reconfiguration is considered together with adjustments of CBs. When two basic loops are allowed to be formed in the system with simultaneous adjustments of CBs, the PV penetration can be increased in 13.71% in relation to the initial configuration of Case I, to 15,710.26 kW. As a result, it can be verified that network reconfiguration combined with CBs operation adjustments can provide more versatile solutions to the problem.

The obtained results show that for the 25-node system, the optimal number of loops that allow the maximum PV penetration in the system is two. To validate this, we force the formation of three loops in the system, i.e., all the switches are closed. In this case, results reveal that the PV penetration values are lower than the values with two loops. This apparently contradictory result is explained by the necessity of satisfying both Kirchhoff's laws in the system: an additional closed circuit improves the capacity of the system for complying with Kirchhoff's current law, but additional loops are formed, and Kirchhoff's voltage law must be satisfied in all loops, leading to a more constrained problem. This phenomenon is known as Braess's paradox, and more information about it can be found in [18] for the optimal transmission switching problem.

IV. Conclusions

This study presented a stochastic scenario-based mixed-integer linear programming model for the problem of short-term planning of three-phase unbalanced distribution systems to increase the network's photovoltaic (PV) generation hosting capacity through network reconfiguration and capacitor banks (CBs) operation. Both radial and closed-loop operations are considered in the network reconfiguration.

When reconfiguration with closed-loop topologies was examined with simultaneous adjustments of CBs operation, the obtained results indicated a greater capacity for PV generation penetration. As a result, the presented approach can provide more environmentally friendly and efficient operating schemes while deferring the need for network structure reinforcement investments.

An important conclusion of this study is that not necessarily an operation configuration with all switches closed is the topology with higher PV generation hosting capacity values. As seen in the obtained results, the total PV generation installed usually increases as the number of basic loops increases. However, due to Braess's paradox, additional closed switches may lead to lower-quality solutions.

Future works could include voltage control through other devices, such as on-load tap changers and voltage regulators for increasing the PV hosting capacity of distribution systems.

TABLE II
Results for the 25-Node Network – Case I: Without Considering Network Reconfiguration and CB Adjustment

Results	Radial	1 Loop	2 Loops	3 Loops
Total PV generation installed (kW)	13,816.14	14,431.95	15,073.42	14,942.76
PV generation installed at nodes 11/15/18 (kW)	3,490.30/ 3,426.41/ 6,899.42	2,950.93/ 4,584.97/ 6,896.04	1,368.73/ 6,884.40/ 6,820.29	1,523.63/ 6,821.61/ 6,597.53
Open switches	5-22, 15-8, 12-25	5-22, 12-25	5-22	–
CB modules connected at nodes 5/14/25 phase (a,b,c)	5-(2,2,2)/ 14-(2,2,2)/ 25-(2,2,2)	5-(2,2,2)/ 14-(2,2,2)/ 25-(2,2,2)	5-(2,2,2)/ 14-(2,2,2)/ 25-(2,2,2)	5-(2,2,2)/ 14-(2,2,2)/ 25-(2,2,2)
Total emissions (tonnes)	25,792.82	25,533.69	25,224.21	25,249.99

TABLE III
Results for the 25-Node Network – Case II: Without Considering Network Reconfiguration and Considering CB Adjustment

Results	Radial	1 Loop	2 Loops	3 Loops
Total PV generation installed (kW)	14,151.95	14,855.11	15,554.29	15,314.56
PV generation installed at nodes 11/15/18 (kW)	3,774.44/ 3,451.67/ 6,925.83	2,499.93/ 5,447.41/ 6,907.77	1,429.41/ 7,172.70/ 6,952.19	1,669.58/ 6,936.90/ 6,708.10
Open switches	5-22, 15-8, 12-25	5-22, 12-25	5-22	–
CB modules connected at nodes 5/14/25 phase (a,b,c)	5-(0,0,2)/ 14-(2,2,2)/ 25-(1,0,2)	5-(0,0,2)/ 14-(1,1,2)/ 25-(0,0,2)	5-(0,0,1)/ 14-(0,0,2)/ 25-(0,0,1)	5-(2,1,0)/ 14-(0,0,2)/ 25-(1,1,2)
Total emissions (tonnes)	25,665.79	25,431.13	25,226.86	25,188.07

TABLE IV
Results for the 25-Node Network – Case III: Considering Network Reconfiguration and not Considering CB Adjustment

Results	Radial	1 Loop	2 Loops	3 Loops
Total PV generation installed (kW)	14,793.34	15,308.86	15,346.71	14,942.76
PV generation installed at nodes 11/15/18 (kW)	3,200.07/ 4,568.70/ 7,024.56	1,689.00/ 6,599.96/ 7,019.91	1,500.07/ 6,846.80/ 6,999.83	1,523.63/ 6,821.61/ 6,597.53
Open switches	4-5, 14-15, 23-24	4-5, 9-10	4-5	–
CB modules connected at nodes 5/14/25 phase (a,b,c)	5-(2,2,2)/ 14-(2,2,2)/ 25-(2,2,2)	5-(2,2,2)/ 14-(2,2,2)/ 25-(2,2,2)	5-(2,2,2)/ 14-(2,2,2)/ 25-(2,2,2)	5-(2,2,2)/ 14-(2,2,2)/ 25-(2,2,2)
Total emissions (tonnes)	25,529.62	25,219.88	25,177.16	25,249.99

TABLE V
Results for the 25-Node Network – Case IV: Considering Both Network Reconfiguration and CB Adjustment

Results	Radial	1 Loop	2 Loops	3 Loops
Total PV generation installed (kW)	14,971.44	15,625.47	15,710.26	15,314.56
PV generation installed at nodes 11/15/18 (kW)	2,910.89/ 5,003.80/ 7,056.75	1,536.18/ 6,997.88/ 7,091.41	1,532.75/ 7,043.77/ 7,133.75	1,669.58/ 6,936.90/ 6,708.10
Open switches	4-5, 7-14, 23-24	4-5, 10-11	4-5	–
CB modules connected at nodes 5/14/25 phase (a,b,c)	5-(2,1,2)/ 14-(0,0,2)/ 25-(2,2,1)	5-(0,0,2)/ 14-(0,0,2)/ 25-(1,1,1)	5-(0,0,1)/ 14-(0,0,2)/ 25-(0,0,1)	5-(2,1,0)/ 14-(0,0,2)/ 25-(1,1,2)
Total emissions (tonnes)	25,461.82	25,189.13	25,199.57	25,188.07

References

[1] Y. Y. Fu and H. D. Chiang, "Toward optimal multiperiod network reconfiguration for increasing the hosting capacity of distribution networks," *IEEE Trans. Power Deliv.*, vol. 33, no. 5, pp. 2294–2304, Oct. 2018.

[2] F. Capitanescu, L. F. Ochoa, H. Margossian, and N. D. Hatziargyriou, "Assessing the potential of network reconfiguration to improve distributed generation hosting capacity in active distribution systems," *IEEE Trans. Power Syst.*, vol. 30, no. 1, pp. 346–356, 2015.

[3] R. A. Jacob and J. Zhang, "Distribution network reconfiguration to increase photovoltaic hosting capacity," in *2020 IEEE Power & Energy Society General Meeting*, 2020, pp. 1–5.

[4] M. Lavorato, J. F. Franco, M. J. Rider, and R. Romero, "Imposing radiality constraints in distribution system optimization problems," *IEEE Trans. Power Syst.*, vol. 27, no. 1, pp. 172–180, Feb. 2012.

[5] D. Ritter, J. F. Franco, and R. Romero, "Analysis of the radial operation of distribution systems considering operation with minimal losses," *Int. J. Electr. Power Energy Syst.*, vol. 67, pp. 453–461, May 2015.

[6] T.-H. Chen, W.-T. Huang, J.-C. Gu, G.-C. Pu, Y.-F. Hsu, and T.-Y. Guo, "Feasibility study of upgrading primary feeders from radial and open-loop to normally closed-loop arrangement," *IEEE Trans. Power Syst.*, vol. 19, no. 3, pp. 1308–1316, Aug. 2004.

[7] R. Vargas, L. H. Macedo, J. M. Home-Ortiz, and R. Romero, "Optimal restoration of distribution systems considering temporary closed-loop operation," *IEEE Syst. J.*, pp. 1–12, 2021.

[8] M. R. M. Cruz, D. Z. Fitiwi, S. F. Santos, S. J. P. S. Mariano, and J. P. S. Catalão, "Prospects of a meshed electrical distribution system featuring large-scale variable renewable power," *Energies*, vol. 11, no. 12, Dec. 2018.

[9] M. Davoudi, V. Cecchi, and J. R. Aguero, "Network reconfiguration with relaxed radiality constraint for increased hosting capacity of distribution systems," in *2016 IEEE Power and Energy Society General Meeting*, 2016, pp. 1–5.

[10] M. S. S. Abad and J. Ma, "Photovoltaic hosting capacity sensitivity to active distribution network management," *IEEE Trans. Power Syst.*, vol. 36, no. 1, pp. 107–117, Jan. 2021.

[11] S. Wang, S. Chen, L. Ge, and L. Wu, "Distributed generation hosting capacity evaluation for distribution systems considering the robust optimal operation of OLTC and SVC," *IEEE Trans. Sustain. Energy*, vol. 7, no. 3, pp. 1111–1123, Jul. 2016.

[12] F. Ding and B. Mather, "On distributed PV hosting capacity estimation, sensitivity study, and improvement," *IEEE Trans. Sustain. Energy*, vol. 8, no. 3, pp. 1010–1020, Jul. 2017.

[13] J. F. Franco, M. J. Rider, and R. Romero, "A mixed-integer linear programming model for the electric vehicle charging coordination problem in unbalanced electrical distribution systems," *IEEE Trans. Smart Grid*, vol. 6, no. 5, pp. 2200–2210, Sep. 2015.

[14] S. Pfenninger and I. Staffell, "Renewables.ninja," 2020. [Online]. Available: https://www.renewables.ninja/. [Accessed: 01-Nov-2020].

[15] J. M. Home-Ortiz, M. Pourakbari-Kasmaei, M. Lehtonen, and J. R. Sanches Mantovani, "Optimal location-allocation of storage devices and renewable-based DG in distribution systems," *Electr. Power Syst. Res.*, vol. 172, pp. 11–21, Jul. 2019.

[16] R. Fourer, D. M. Gay, and B. W. Kernighan, *AMPL: A modeling language for mathematical programming*, 2nd ed. Duxbury, MA, USA: Thomson, 2003.

[17] IBM, "IBM ILOG CPLEX Optimization Studio 20.1.0 documentation," *2021*. [Online]. Available: https://www.ibm.com/support/knowledgecenter/SSSA5P_20.1.0/COS_KC_home.html. [Accessed: 01-Feb-2021].

[18] M. Flores, L. H. Macedo, and R. Romero, "Alternative mathematical models for the optimal transmission switching problem," *IEEE Syst. J.*, vol. 15, no. 1, pp. 1245–1255, Mar. 2021.